nature communications

Article

https://doi.org/10.1038/s41467-025-64144-0

ALKBH8-mediated codon-specific translation promotes colorectal tumorigenesis

Received: 24 October 2024

Accepted: 10 September 2025

Published online: 13 October 2025

Check for updates

Yu Qian[1,4], Canlan Wu[1,4], Saisai Wei[2,4], Sujun Yan[1], Junxuan Peng[1], Lei Yu[1], Yunyi Gao[1], Jingyu Hou[1], Wentao Yu[1], Zhanghui Chen[3] ✉, Jun Zhang[1] ✉ & Xiangwei Gao[1] ✉

Reprogramming gene expression at the translational level drives intestinal tumorigenesis. Codon decoding during translation elongation relies on tRNA modifications, while their pathological relevance in colorectal cancer remains to be elucidated. Here, we show that AlkB homolog 8 (ALKBH8), a uridine 34 (U34) tRNA methyltransferase, is a direct target of Wnt/β-catenin and is upregulated in colorectal cancer. Genetic ablation of ALKBH8 inhibits the development of intestinal tumors in $Apc^{min/+}$, azoxymethane/dextran sulfate sodium (AOM/DSS), and xenograft models. Loss of ALKBH8 induces ribosome pausing at adenine-ending codons, impairing the translation elongation of mRNAs enriched with these codons. Specifically, ALKBH8 regulates the translation of *KRAS* proto-oncogene in a codon-dependent manner. Rescue experiments demonstrate that the methyltransferase activity of ALKBH8 is required for its translation-promoting function. Together, our findings reveal ALKBH8-dependent mRNA translation as a critical mediator of intestinal tumorigenesis, underscoring its potential as a promising target for colorectal cancer therapy.

Colorectal cancer (CRC), one of the deadliest cancers worldwide, arises from stepwise accumulation of genetic and epigenetic perturbations that stimulate oncogenic pathways[1,2]. The aberrant activation of β-catenin (CTNNB1) signaling is recognized as the key event in the development of CRC[3,4]. In normal intestinal epithelial cells, β-catenin is targeted by adenomatous polyposis coli (APC) for degradation. Inactivating mutations in *APC* or activating mutations in *CTNNB1*, which frequently happen in CRC tissue, lead to the stabilization of β-catenin[5]. The subsequent translocation of β-catenin to the nucleus promotes the transcription of oncogenes such as *c-Myc*, driving intestinal tumorigenesis[3,4,6]. In addition to transcriptional control, accumulating evidence indicates that reprogramming of gene expression at the translational level is required for intestinal tumorigenesis[7–9], while our understanding of this process is still limited.

The epitranscriptomic code generated by RNA modifications embeds an important layer of gene expression regulation beyond the primary sequence[10]. Transfer RNAs (tRNAs) are the most heavily modified RNA species concerning number, density, and diversity. In particular, the wobble uridine (U34) frequently carries chemical modifications that are functionally important for mRNA translation[11]. The enzymatic cascade catalyzing U34 modifications includes the acetyltransferase elongators (ELPs), the ALKBH8, and the ubiquitin-related modifier 1 (URM1) pathway enclosing the cytosolic thiouridylase homolog 1/2 (CTU1/CTU2). ELPs catalyze the formation of 5-carbamoylmethyluridine (cm5U), while ALKBH8 uses cm5U as a

[1]Department of Clinical Laboratory of Sir Run Run Shaw Hospital, School of Public Health, Zhejiang University School of Medicine, Hangzhou, China. [2]Key Laboratory of Laparoscopic Technology of Zhejiang Province, Department of General Surgery, Sir Run-Run Shaw Hospital, Zhejiang University School of Medicine, Hangzhou, China. [3]Zhanjiang Institute of Clinical Medicine, Zhanjiang Central Hospital, Zhanjiang, China. [4]These authors contributed equally: Yu Qian, Canlan Wu, Saisai Wei. ✉e-mail: zjcell@126.com; jameszhang2000@zju.edu.cn; xiangweigao@zju.edu.cn

substrate to subsequently catalyze the formation of 5-methoxycarbonylmethyluridine (mcm5U) in tRNAs including $tRNA^{Lys(UUU)}$, $tRNA^{Gln(UUG)}$, $tRNA^{Glu(UUC)}$, $tRNA^{Arg(UCU)}$ and $tRNA^{Gly(UCC)}$. The wobble uridine in $tRNA^{Lys(UUU)}$, $tRNA^{Gln(UUG)}$ and $tRNA^{Glu(UUC)}$ could be further catalyzed by the URM1 pathway to add 2-thiouridine (s2U) modification[12–14]. Studies in a variety of model organisms have shown that U34 modifications, including s2U and mcm5U, are required for the efficient decoding of AA-ending codons (GAA, CAA, and AAA) by refining U34 recognition[15,16].

In addition to catalyzing mcm5U formation, the ALKBH8 protein has several other functions. First, the AlkB domain of ALKBH8 could hydroxylate mcm5U into 5-methoxycarbonylhydroxymethyluridine (mchm5U), which is specific to $tRNA^{Gly(UCC)}$[17,18]. Second, ALKBH8 is essential for mcm5U and mcm5Um modifications at the wobble position of selenocysteine tRNA ($tRNA^{UGA-SEC}$), necessary for the recoding of the UGA stop codon of selenocysteine-containing proteins[19]. Notably, these two activities of ALKBH8 are specific to mammalian cells and do not occur in budding yeast. Although studies have indicated that its yeast homolog Trm9 selectively regulates the decoding of AGA and GAA codons[20,21], the role of mammalian ALKBH8 in translation elongation has yet to be explored.

Recent studies have highlighted an important role of U34 tRNA cascade in cancer development. ELPs and CTU1/2 are upregulated in colon adenocarcinoma and breast cancer. By regulating codon usage and thereby increasing the expression of specific oncogenes, these enzymes sustain malignant transformation[22], cancer cell metastasis[23], chemotherapy resistance[16], and macrophage polarization[24]. However, germline loss-of-function mutations in ELP1 have been identified to be a determinant in the pathogenesis of Sonic Hedgehog medulloblastoma[25], indicating the complex function of U34 enzymes in cancer development. Few studies indicated that ALKBH8 promotes bladder cancer progression[26,27], while its role in other cancers remains poorly characterized.

In this study, we have identified ALKBH8 as a direct target of β-catenin that mediates intestinal tumorigenesis. Using ribosome profiling, we found that loss of ALKBH8 in CRC cells results in ribosome pausing at several adenine(A)-ending codons, impairing the translation elongation of a subset of mRNAs. These findings define ALKBH8 as a translation regulator in the promotion of colorectal tumorigenesis.

Results

The transcription of ALKBH8 is regulated by β-catenin and is upregulated in CRC

To identify the direct targets of β-catenin, we knocked down β-catenin and performed RNA-seq in colorectal cancer cell line HCT116, harboring a constitutively activating mutation of β-catenin (Data S1)[28]. By combining with the published β-catenin ChIP-seq data[29], we identified 168 down-regulated genes upon β-catenin knockdown with direct β-catenin binding (Fig. 1a). Among these genes, we focused on RNA modification enzymes, with ALKBH8 showing a relatively large change and its oncogenic role remaining largely unexplored (Data S1). Independent ChIP-qPCR analysis confirmed the direct binding of β-catenin with ALKBH8 promoter (Fig. 1b). Knockdown of β-catenin in HCT116 cells inhibited ALKBH8 expression at both mRNA and protein levels (Figs. 1c, d). Reciprocally, expression of a non-degradable β-catenin into RKO cells, whose APC/β-catenin pathway is intact, increased ALKBH8 expression (Figs. 1e, f). β-Catenin forms a complex with TCF4 and binds DNA through the core TCF4 motif TCAAAG. ALKBH8 gene proximal promoter contains a consensus TCF4 motif (Fig. 1g, Fig. S1a). To determine the direct regulation of β-catenin on ALKBH8 transcription, the luciferase reporters containing ALKBH8 promoter sequence or TCF4-motif-deleted sequence were used. Wild-type ALKBH8 promoter activity was significantly induced following β-catenin expression. However, deletion of TCF4 motif abolished β-catenin effect, implying that ALKBH8 promoter activity is β-catenin-dependent (Fig. 1h). Collectively, our data demonstrated that ALKBH8 is a direct target of β-catenin.

Since mutations in WNT/β-catenin pathway account for about 90% of CRC[7,30], we examined whether ALKBH8 expression was altered in mouse and human intestinal tumors. High ALKBH8 expression was observed in intestinal adenomas but not in adjacent normal tissue from $Apc^{min/+}$ as well as azoxymethane (AOM)/dextran sulfate sodium (DSS)-induced mouse intestinal tumor model (Figs. 1i, j). TCGA datasets revealed upregulation of ALKBH8 expression in CRC (Fig. 1k). Moreover, *ALKBH8* mRNA level showed positive correlation with *CTNNB1* expression (Fig. 1l), supporting the regulating effect by β-catenin. Together, these results suggested that an increase of ALKBH8 might play an oncogenic role in intestinal tumorigenesis.

ALKBH8 is essential for intestinal epithelial proliferation

To address where ALKBH8 is expressed in the intestine, we queried the Human Protein Atlas and found that ALKBH8 is broadly expressed across various segments of the human intestine. Immunofluorescence (IF) analysis confirmed the widespread expression of ALKBH8 protein in epithelial cells of the duodenum, jejunum, ileum, and colon, with predominant cytoplasmic localization (Fig. 2a). To examine which epithelial subtypes express ALKBH8, we analyzed the single-cell RNA sequencing data from mouse small intestine and colon. The results showed that ALKBH8 is expressed across multiple intestinal epithelial subtypes, including stem cells, transit-amplifying (TA) cells, and differentiated lineages (Fig. S1b). We validated these findings through IF experiments, which revealed co-expression of ALKBH8 with LGR5 (stem cells), LYZ (paneth cells), Ki67 (proliferating cells), MUC2 (goblet cells), and DCLK1 (tuft cells) (Fig. 2b).

To assess the function of ALKBH8 in intestinal epithelium, we generated intestinal epithelial cell-specific conditional knock out mouse for *Alkbh8* ($Alkbh8^{cKO}$) (Fig. 2c). The ablation of *Alkbh8* gene did not affect the intestinal architecture, indicating that ALKBH8 is largely dispensable for intestinal homeostasis under physiological condition. BrdU+ cells, which are mainly proliferating intestinal stem cells and transit-amplifying cells, were slightly decreased in $Alkbh8^{cKO}$ mice (Figs. 2d, e). To comprehensively assess changes in epithelial lineage differentiation, we determined the expression of cell subtype-specific markers. A decrease in Ki67 expression suggested reduced proliferation. Lgr5 expression was reduced in $Alkbh8^{cKO}$ intestines, indicating impaired stem cell maintenance. In contrast, the expression levels of *Lyz1* (paneth cells), *Muc2* (goblet cells), and *Dclk1* (tuft cells) were elevated, indicating enhanced differentiation of specific epithelial lineages upon ALKBH8 loss (Fig. S1c–e). Together, these findings indicate that ALKBH8 preserves intestinal epithelial stemness and proliferative capacity.

We further studied the function of ALKBH8 in epithelial regeneration using DSS-induced colitis model. The colon length was markedly reduced in $Alkbh8^{cKO}$ mice (Fig. S1f). Hematoxylin & eosin staining revealed markedly aggravated ulcer formation in $Alkbh8^{cKO}$ colon (Figs. S1g, h). $Alkbh8^{cKO}$ mice displayed significantly higher levels of pro-inflammatory cytokines, including Ccl2, Il6, S100a8 and Tnfα (Fig. S1i). Together, these findings demonstrate that epithelial-specific loss of ALKBH8 aggravates inflammation, indicating that ALKBH8 is essential for effective epithelial regeneration.

Alkbh8 deletion reduces murine intestinal tumorigenesis

Given the upregulation of ALKBH8 in intestinal tumors, we examined the function of ALKBH8 in β-catenin-driven tumorigenesis using the $Apc^{min/+}$ mouse model. Deletion of ALKBH8 dramatically reduced intestinal tumor formation. The tumor number was significantly diminished in $Alkbh8^{cKO}$ mice (Fig. 3a, Fig. S2a). Most of the tumors in $Alkbh8^{cKO}$ mice were smaller in size compared to the control group. *Alkbh8* deficiency in the $Apc^{min/+}$ background does not lead to splenomegaly (Fig. S2b). Moreover, *Alkbh8* depletion significantly extended

https://doi.org/10.1038/s41467-025-64144-0

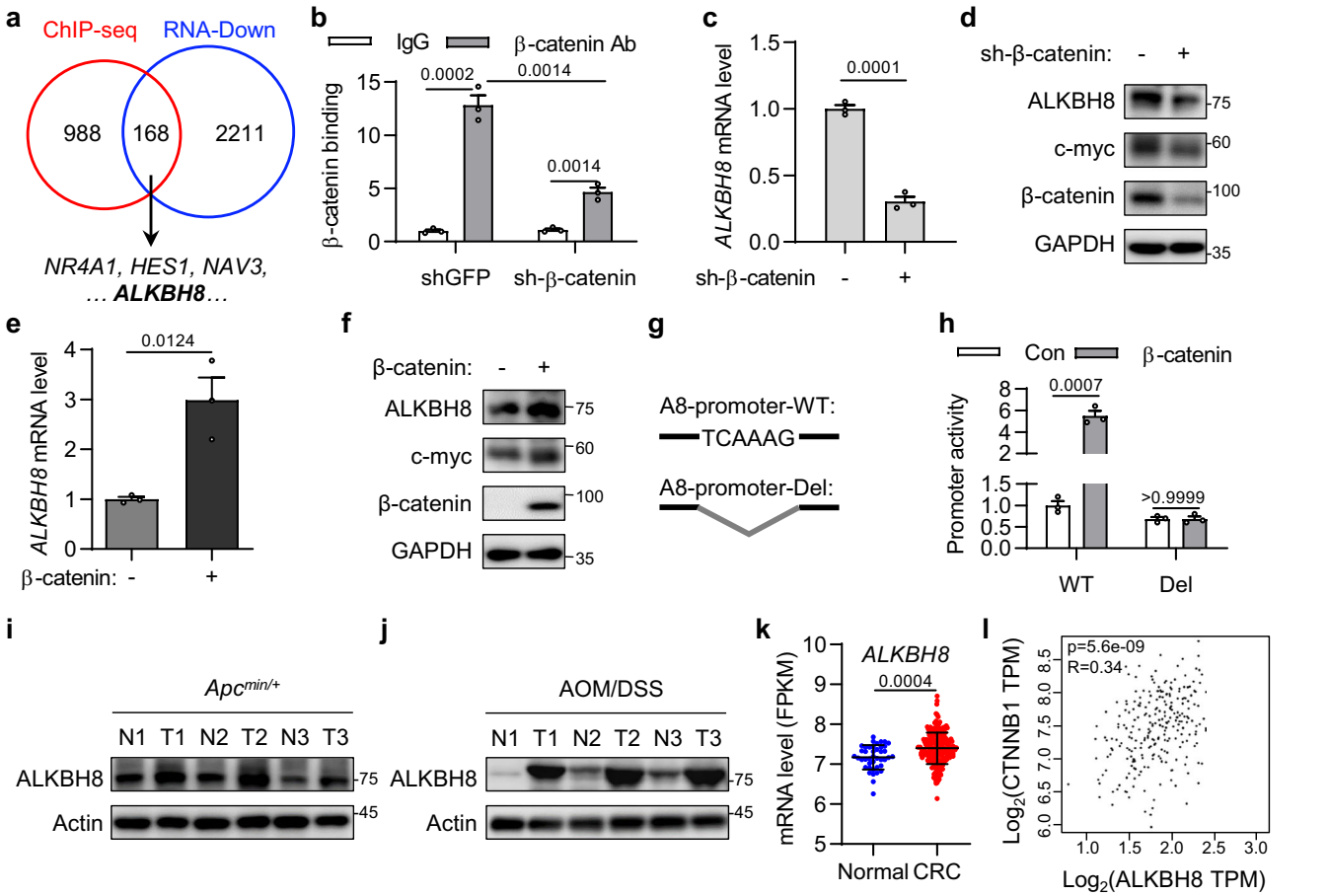

Fig. 1 | β-Catenin promotes the expression of *ALKBH8*. **a** Venn diagram demonstrating the overlap of down-regulated genes in *β-catenin* knockdown cells and β-catenin-binding targets. **b** ChIP-qPCR analysis of β-catenin binding to ALKBH8 gene promoter region, with *β-actin* (*ACTB*) gene serving as the control. ChIP analysis was performed with antibodies against β-catenin or control IgG and analyzed by qPCR. Mean ± SEM, 3 biological replicates, two-sided *t*-test. **c**, **d** The mRNA level (**c**) and protein level (**d**) of ALKBH8 in HCT116 cells with or without β-catenin knockdown. Mean ± SEM, 3 biological replicates, two-sided *t*-test. The samples derive from the same experiment but different gels for ALKBH8, c-myc, and GAPDH, and another for β-catenin were processed in parallel. **e**, **f** The mRNA level (**e**) and protein level (**f**) of ALKBH8 in RKO cells with or without β-catenin overexpression. Mean ± SEM, 3 biological replicates, two-sided *t*-test. The samples derive from the same experiment, but different gels for β-catenin and c-myc, another for ALKBH8 and GAPDH, were processed in parallel. **g** Schematic of luciferase reporters with wild-type ALKBH8 promoter or TCF4 binding site mutated construct. **h** Dual-Luciferase assay using constructs with either the wild-type *ALKBH8* promoter or a mutated TCF4 binding site in HCT116 cells with or without β-catenin overexpression. Mean ± SEM, 3 biological replicates, two-sided *t*-test. **i** ALKBH8 protein expression in intestinal tissue from *Apc*$^{min/+}$ mice. N, normal tissue. T, tumor tissue. **j** ALKBH8 protein expression in intestinal tissue from AOM/DSS-treated mice. N, normal tissue. T, tumor tissue. The samples derive from the same experiment but different gels for ALKBH8, another for Actin were processed in parallel. **k** The mRNA level of *ALKBH8* in colorectal cancer tissues and adjacent normal tissues from TCGA database (normal = 42, CRC = 286). Mean ± SD, two-sided *t*-test. **l** Two-sided Pearson's correlation analysis of *ALKBH8* mRNA and *CTNNB1* mRNA in colorectal cancer tissues from TCGA database, 268 samples. Source data are provided as a Source Data file.

the lifespan of *Apc*$^{min/+}$ mice (Fig. S2c, d). To address whether *Alkbh8* deficiency in epithelial stem cells impairs Wnt-driven tumor initiation, we knocked down *Alkbh8* in organoids from *Apc*$^{F/F}$*;Lgr5-EGFP-IRES-CreERT2* mice. Tumor organoids formed "spheroids" structure, and exhibited reduced diameter and slower growth upon *Alkbh8* knockdown (Figs. S2e), indicating that ALKBH8 in stem cells contributes to tumorigenesis.

To further confirm the results in *Apc*$^{min/+}$ mouse model, we employed AOM/DSS-induced tumor model (Fig. 3b). In this model, mice develop CRC as the result of mutations in several genes including β-catenin[31]. Decreased tumor number and tumor size were detected in *Alkbh8*^{cKO} mice compared to the wild-type group (Fig. 3c, e). Single-cell RNA sequencing revealed that *Alkbh8*^{cKO} tumors exhibited a substantial reduction in malignant epithelial cells, along with decreased infiltration of neutrophils. In contrast, T cells and B cells were increased. Within the T cell compartment, cytotoxic CD8$^+$ Gzma$^+$ T cells and proliferative CD8$^+$ Mki67$^+$ T cells were enriched, while Foxp3$^+$ regulatory T cells (Tregs) were diminished, reflecting a shift toward a less immunosuppressive T cell landscape (Fig. S2f–h). Moreover, there was a notable shift in macrophage polarization toward a pro-inflammatory M1 phenotype, and a concomitant decrease in anti-inflammatory M2 macrophages (Fig. S2i). Immunofluorescence staining confirmed a reduction in total macrophages and M2 macrophages (CD163$^+$), accompanied by an increase in M1 macrophages (CD86$^+$) in cKO mice (Fig. S2j). Together, these data highlighted the necessity of ALKBH8 in intestinal tumorigenesis in mice. We observed reduced expression of *Lgr5*, *β-catenin*, and *Olfm4* in *Alkbh8*^{cKO} tumors from both *Apc*$^{min/+}$ model and AOM/DSS model, indicating a role of ALKBH8 in Wnt signaling activation (Fig. S2k–m).

ALKBH8 promotes the development of human colorectal cancer in vitro and in vivo

To determine the role of ALKBH8 in human CRC development, we knocked out *ALKBH8* gene in HCT116 cells (Fig. 3f). Knockout of ALKBH8 significantly reduced cell proliferation and colony formation in soft agar, while increasing Annexin V$^+$ cells (Fig. 3g–j). To determine

https://doi.org/10.1038/s41467-025-64144-0

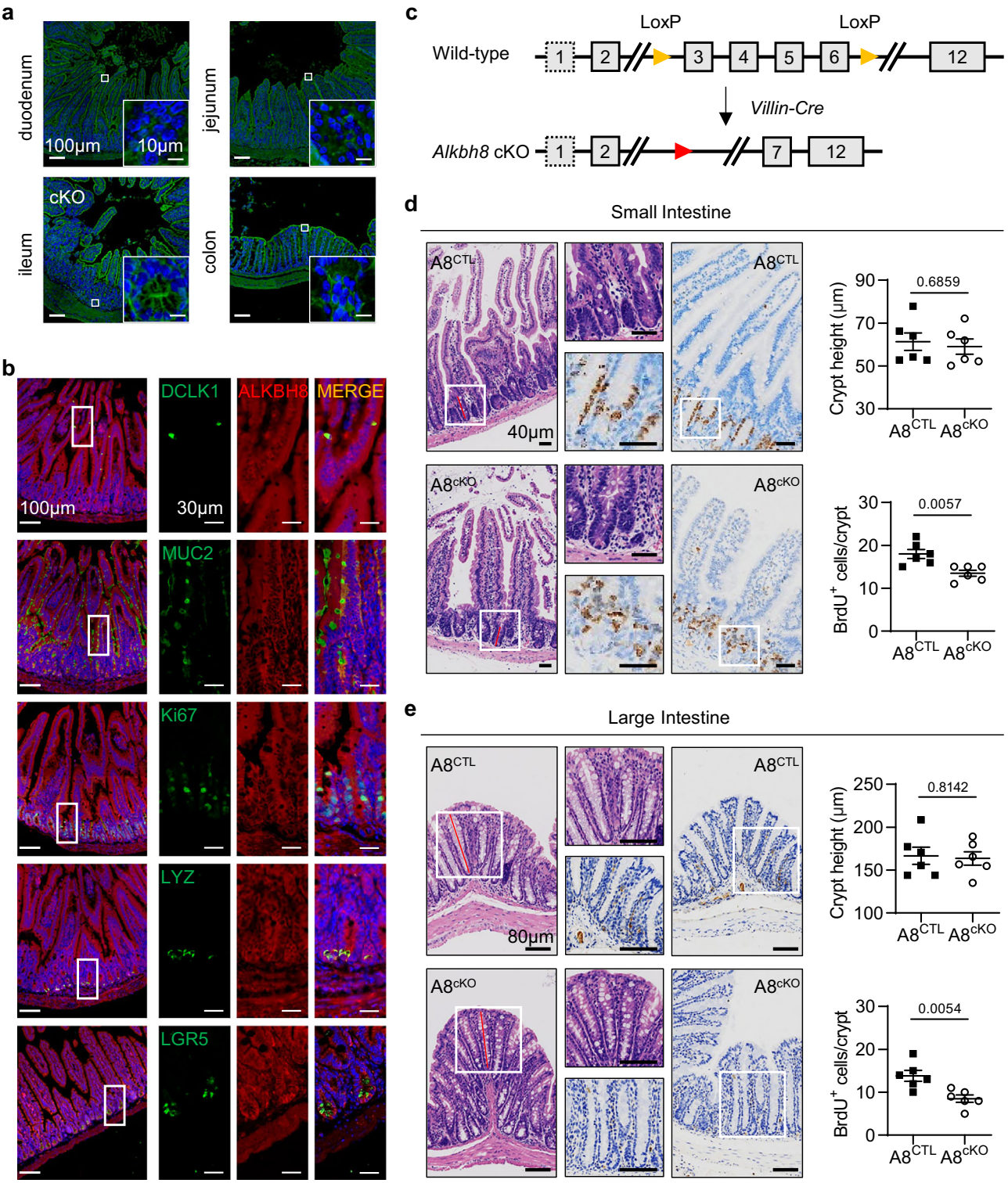

Fig. 2 | Depletion of Alkbh8 reduces intestinal epithelium proliferation. **a** Immunofluorescence staining of ALKBH8 in duodenum, jejunum, ileum, and colon sections of mice. **b** Immunofluorescence co-staining of ALKBH8 with DCLK1, MUC2, Ki67, LYZ, and LGR5 in duodenum sections of mice. **c** Schematic of *Alkbh8* conditional knockout (*Alkbh8*^{cKO}) mouse. **d** The representative jejunum from wild-type (*Alkbh8*^{CTL}) and *Alkbh8*^{cKO} mice. Left: hematoxylin and eosin staining (H&E); middle: BrdU staining; right: quantification of crypt height and BrdU+ cells. **e** The representative colon from wild-type (*Alkbh8*^{CTL}) and *Alkbh8*^{cKO} mice. Left: hematoxylin and eosin staining (H&E); middle: BrdU staining; right: quantification of crypt height and BrdU+ cells. Mean ± SEM, 6 biological replicates, two-sided *t*-test. Source data are provided as a Source Data file.

whether ALKBH8 could directly promote CRC progression, we performed an overexpression experiment. Overexpression of ALKBH8 enhanced HCT116 cell proliferation and colony formation in vitro (Figs. 3k–n). Further, we determined tumor growth in a nude mouse model. Depletion of ALKBH8 significantly suppressed tumor growth, while overexpression of ALKBH8 promoted tumor growth in vivo (Figs. 3o–q). Collectively, these data indicate that ALKBH8 promotes colorectal cancer development.

https://doi.org/10.1038/s41467-025-64144-0

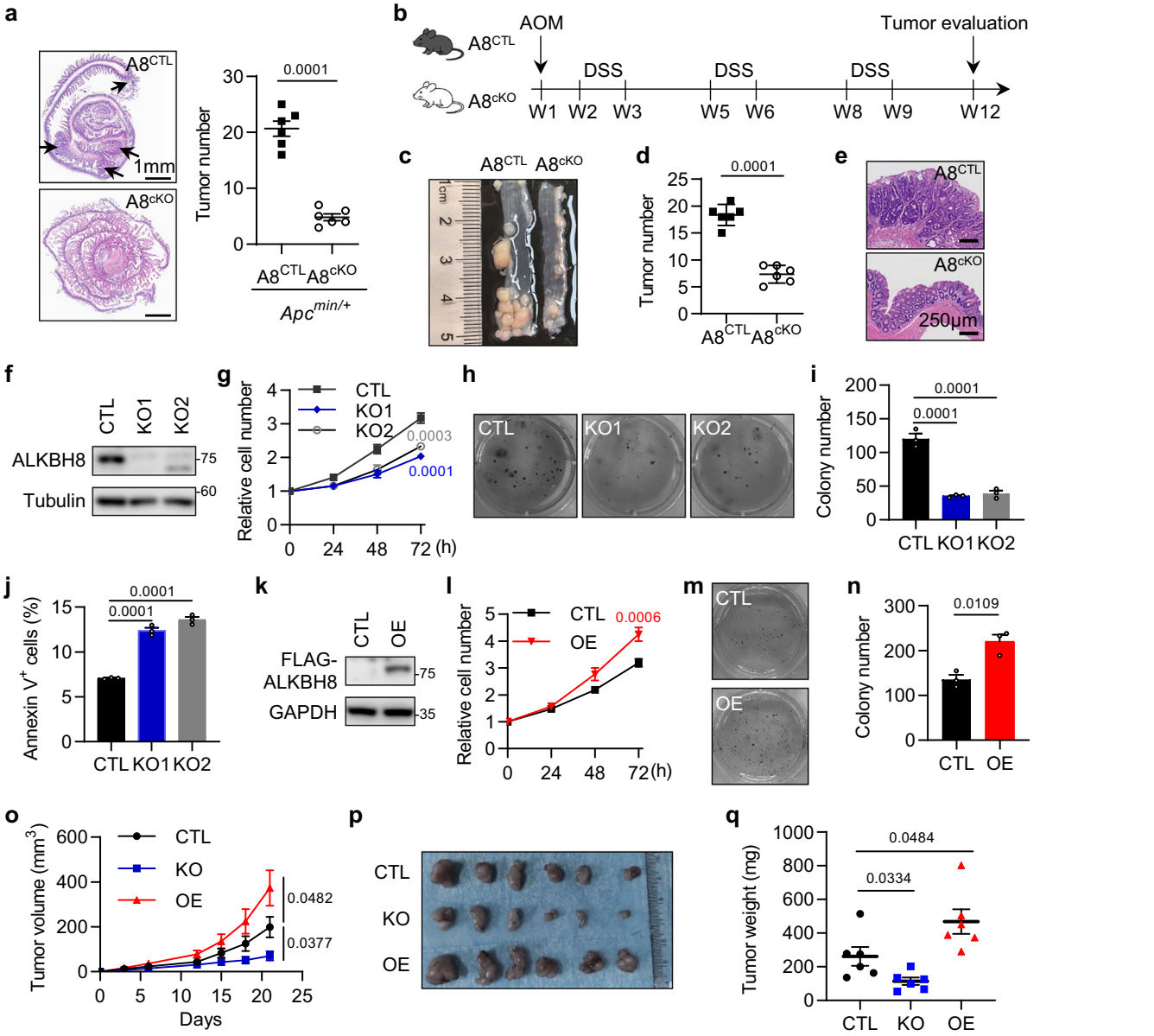

Fig. 3 | ALKBH8 promotes intestinal tumorigenesis. a H&E staining of small intestines from 24-week-old *Apc*$^{min/+}$;*Alkbh8*^{CTL} and *Apc*$^{min/+}$;*Alkbh8*^{cKO} mice. The black arrows indicate the tumors. Statistical analysis of tumor number is shown on the right panel. Mean ± SEM, 6 mice for each group, two-sided *t*-test. **b** Workflow of the AOM/DSS-induced cancer model. **c** Colons from *Alkbh8*^{CTL} and *Alkbh8*^{cKO} mice on day 84 of AOM/DSS induction. **d** Colon tumor number from (**c**). Mean ± SEM, 6 mice for each group, two-sided *t*-test. **e** H&E staining of colons from *Alkbh8*^{CTL} and *Alkbh8*^{cKO} mice after AOM/DSS induction. **f** Immunoblotting analysis of ALKBH8 (A8) expression in CTL and A8-KO HCT116 cells. **g** The proliferation assay of CTL and A8-KO HCT116 cells. Cell number at day 4 was statistically analyzed. Mean ± SEM, 3 biological replicates, one-way ANOVA with Dunnett's multiple comparisons test. **h** Colony formation assay of CTL and A8-KO HCT116 cells. **i** The statistical analysis of colony numbers in (**h**). Mean ± SEM, 3 biological replicates, one-way ANOVA with Dunnett's multiple comparisons test. **j** Apoptosis analysis of CTL, A8-KO HCT116 cells. Mean ± SEM, 3 biological replicates, one-way ANOVA with Dunnett's multiple comparisons test. **k** Immunoblotting analysis of ALKBH8 expression in CTL and A8-OE HCT116 cells. **l** The proliferation assay of CTL and A8-OE HCT116 cells. Cell number at day 4 was statistically analyzed. Mean ± SEM, 3 biological replicates, two-sided *t*-test. **m** Colony formation assay of CTL and A8-OE HCT116 cells. **n** The statistical analysis of colony numbers in (**m**). Mean ± SEM, 3 biological replicates, two-sided *t*-test. **o** The volume of xenograft tumors from mice implanted with CTL, A8-KO, or A8-OE cells. Mean ± SEM, 6 mice for each group, one-way ANOVA with Dunnett's multiple comparisons test. **p** The images of xenograft tumors from mice implanted with CTL, A8-KO, or A8-OE cells. **q** The statistical analysis of tumor weight in (**p**). Mean ± SEM, 6 mice for each group, one-way ANOVA with Dunnett's multiple comparisons test. Source data are provided as a Source Data file.

ALKBH8 deficiency induces codon-dependent translational reprogramming

ALKBH8 catalyzes the formation of 5-methoxycarbonylmethyluridine (mcm5U) at U34 in the anticodon loop of tRNAs. We therefore isolated tRNAs and assessed the level of mcm5U modification in wild-type cells and ALKBH8-KO cells using mass spectrometry. We systematically evaluated the levels of cm5U, mcm5U, and mcm5s2U in both ALKBH8-KO and ALKBH8-OE cells. In ALKBH8-KO cells, we observed a reduction in mcm5U containing modifications, including mcm5U and mcm5s2U, along with an accumulation of cm5U. Conversely, ALKBH8-OE resulted in decreased cm5U and increased mcm5U and mcm5s2U (Fig. 4a). ELP3 depletion completely abolished cm5U, mcm5U, and mcm5s2U levels, confirming that ELP3 is essential for initiating the modification cascade. CTU1 knockdown specifically eliminated mcm5s2U, along with a slight

accumulation of mcm5U and a decrease in cm5U (Fig. S3a). These findings clearly demonstrated the cm5U→mcm5U→mcm5s2U flux.

U34 modifications are required for efficient translation. Thus, we determined the potential effect of ALKBH8 on mRNA translation using OP-puro labeling assay. Data showed that depletion of ALKBH8 reduced global protein synthesis (Fig. 4b). To systematically evaluate the translational changes, we performed ribosome profiling (Ribo-seq) (Fig. 4c). This method has the potential to identify translational changes at single nucleotide resolution. First, we assessed the quality of Ribo-seq data by analyzing several features of ribosome-protected fragments (RPFs). Consistent with previous reports[32,33], the dominant length of RPFs is 28 nt. About 90% of RPFs were mapped to coding sequences (CDSs), and over 85% of RPFs accumulated in the correct frame in our dataset (Fig. S3b). These results suggested that our Ribo-seq data were of high quality and suitable for further analysis.

Aminoacyl-tRNA enters ribosomal A site during elongation. Altered modification in tRNAs may affect aminoacyl-tRNA usage and subsequent ribosome dwell time in A site. We, therefore, analyzed ribosome occupancy in the A site for all the codons. mcm5U was formed in $tRNA^{Lys(UUU)}$, $tRNA^{Gln(UUG)}$, $tRNA^{Glu(UUC)}$, $tRNA^{Arg(UCU)}$ and $tRNA^{Gly(UCC)}$, which might affect the decoding of corresponding codons AAA, CAA, GAA, AGA and GGA. Indeed, ALKBH8-KO cells exhibited increased ribosome density corresponding to these five A-ending codons in the A site, indicating slower translation when these codons are in the ribosomal A site (Fig. 4d). Next, we examined translational changes at the transcript level (Data S2). To that end, all the genes were divided by codon content, and changes in ribosome density upon ALKBH8 knockout were analyzed. For each of these five A-ending codons, codon-rich genes (top 20%) exhibited increased ribosome density while codon-poor genes (bottom 20%) exhibited decreased ribosome density in ALKBH8-KO cells (Fig. S3c). The trend was pronounced when analyzed based on the content of all five A-ending codons (Fig. 4e). To rule out the possibility of changes at the mRNA level, RNA-seq was performed, which showed minimal alterations (Fig. 4f). Relative ribosome density (translation efficiency, TE) was calculated by normalizing Ribo-seq data with RNA-seq data, revealing an increase for A-codon rich genes but a decrease for A-codon poor genes upon ALKBH8 knockout (Fig. 4g). In contrast, the G-ending codons exhibited an opposite trend (Fig. 4h–j). Conversely, ALKBH8 overexpression led to a reduced ribosome density of A-ending codon-rich genes (Fig. S3d). These findings suggest codon-dependent translational reprogramming induced by ALKBH8 depletion.

ALKBH8 regulates the translation elongation of KRAS

To identify ALKBH8-regulated mRNAs, we analyzed genes rich in 5A-ending codons and also exhibited increased ribosome density in ALKBH8-KO cells. Kyoto Encyclopedia of Genes and Genomes (KEGG) pathway enrichment analysis identified the cell cycle pathway as one of the most significantly enriched pathways, which included key genes such as *KRAS* and *CDK1* (Fig. 5a, Data S3). Among these potential candidates, we noticed that proto-oncogene KRAS was listed as the top candidate, having high 5A-ending codons and showing increased ribosome density upon ALKBH8 deletion (Fig. 5b, Data S2). ALKBH8-KO cells exhibited reduced expression of KRAS (Fig. 5c). The mRNA level of KRAS remained unchanged, suggesting that its regulation occurs at the translational level (Fig. 5d). Inhibited expression of KRAS was also observed in the *Alkbh8*-depleted mouse intestinal tumors (Fig. 5e, f). In addition to KRAS, reduced CDK1 expression was also confirmed in ALKBH8-knockout cells (Fig. S4a, b). Knockdown of either ELP3 or CTU1 reduced KRAS protein level, indicating that the three U34 tRNA modifying enzymes are required for efficient KRAS expression (Fig. S4c). HCT116 cells harbor the G13D mutation in *KRAS* gene. To determine whether ALKBH8 regulates *KRAS* translation independently of its mutational status, we conducted experiments in KRAS wild-type RKO cells. In these cells, ALKBH8 knockdown decreased KRAS expression, whereas its overexpression increased KRAS expression (Fig. S4d, e). This observation was further validated in tumor-derived organoids from *$Apc^{F/F}$;Lgr5-EGFP-IRES-CreERT2* mice (Figs. S4f, g). Collectively, these findings suggest that ALKBH8 promotes *KRAS* translation through codon-specific decoding, independent of oncogenic *KRAS* mutations.

To dissect codon dependency, we generated cDNA of a *KRAS* mutant (KRAS-Mut) in which ALKBH8-regulated codons (AAA, CAA, GAA, AGA and GGA) were replaced by their synonymous codons (AAG, CAG, GAG, AGG and GGG) (Fig. 5g). Remarkably, wild-type KRAS (KRAS-WT) expression was downregulated in ALKBH8-KO cells and upregulated in ALKBH8-OE cells, whereas KRAS-Mut expression remained unchanged (Fig. 5h, i, Figs. S4h, j). These data indicated that ALKBH8 directly regulates *KRAS* mRNA translation through specific codon decoding.

To determine whether ALKBH8 regulates translation elongation, we performed a pulse-chase experiment. Translation initiation was inhibited by harringtonine and the run-off of elongating ribosomes was determined by polysome profiling[32,33]. Data revealed that the polysomes (elongating ribosomes) in ALKBH8-KO cells dissociated much more slowly than those in control cells (Figs. 5j, k). We further determined the distribution of *KRAS* mRNAs in each fraction. With harringtonine treatment, the *KRAS* mRNAs dissociated from the polysome fractions in control cells but still accumulated in the polysome fractions of ALKBH8-KO cells (Fig. 5l, m). These results were further confirmed in RKO cells (Fig. S4k–n), suggesting that ALKBH8 deficiency impairs translation elongation.

The methyltransferase domain is required for ALKBH8-regulated translation

ALKBH8 contains an RNA recognition binding motif, an active 2-oxoglutarate-Fe(II) oxygenase (AlkB) domain, and a Class I S-adenosyl-L-methionine (SAM)-dependent methyltransferase (MT) domain (Fig. 6a)[19]. The MT domain catalyzes the mcm5U formation. To discriminate whether mcm5U modification is required for ALKBH8-regulated translation, we mutated the key amino acids in MT domain. Rescue experiments were performed in ALKBH8-KO cells by reconstituting wild-type ALKBH8 or the MT domain mutant. The impaired mcm5U level, global mRNA translation, KRAS expression, cell proliferation and colony formation in ALKBH8-KO cells could be rescued by wild-type ALKBH8 but not the MT domain mutant (Fig. 6b–f), implying that ALKBH8 regulates mRNA translation through mcm5U modification.

KRAS contributes to ALKBH8-mediated cell cycle progression

A key function of KRAS is the activation of cyclinD:CDK4/6, resulting in G1/S phase transition[34,35]. Therefore, we investigated the functional relationship between KRAS and ALKBH8 in cell cycle progression. As expected, knockdown of KRAS increased the proportion of G1 phase cells and decreased the proportion of S phase cells (Fig. 7a–c). This was also observed in ALKBH8 knockout cells, phenocopying KRAS knockdown (Figs. 7d–f). Overexpression of the synonymous KRAS mutant rescued G1 phase arrest in ALKBH8-KO cells (Figs. 7d–f). Consistently, the in vivo tumor growth suppressed by ALKBH8 deficiency was restored by KRAS (Figs. 7g–i). These results suggested that KRAS is a functional target of ALKBH8, facilitating G1/S phase transition in CRC development.

Finally, we assessed the expression of ALKBH8 and KRAS in cancer tissues and paired normal tissues in a cohort of 80 cases of CRC patients. Both ALKBH8 and KRAS showed significant upregulation in CRC tissues (Figs. 7j, k). In accordance with its regulatory role in KRAS translation, ALKBH8 expression was positively correlated with KRAS expression in CRC samples (Fig. 7l).

https://doi.org/10.1038/s41467-025-64144-0

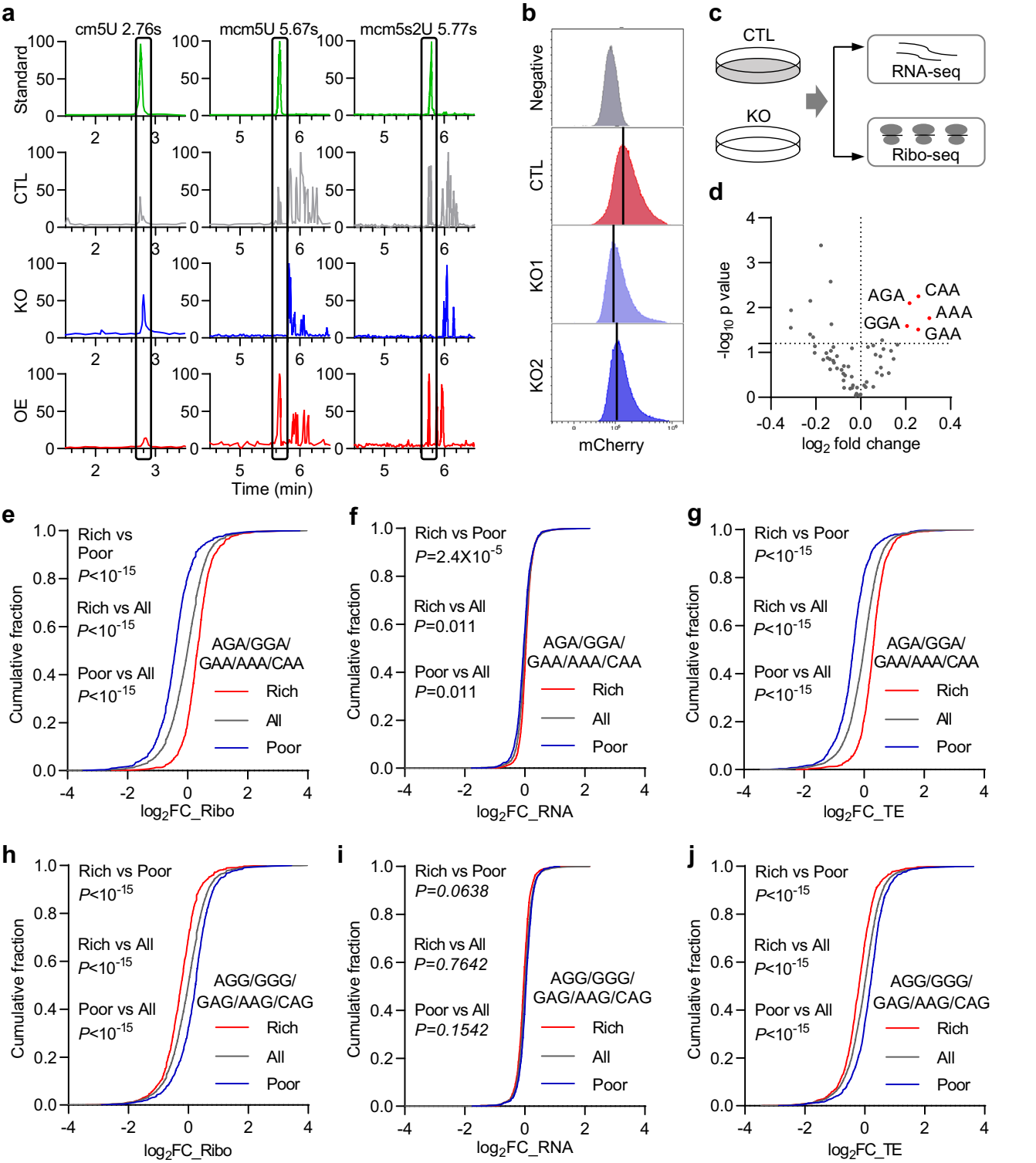

Fig. 4 | Transcriptome-wide identification of ALKBH8-regulated mRNAs. a Mass spectrometry analysis of cm5U, mcm5U and mcm5s2U levels in tRNAs from CTL, A8-KO and A8-OE HCT116 cells, 3 biological replicates. **b** OP-Puro labeling of global translation levels in CTL and A8-KO HCT116 cells, 3 biological replicates. **c** Schematic of RNA-seq (up) and Ribo-seq (bottom) experiments. **d** Fold change of ribosome density in A site for each codon after ALKBH8 depletion. 2 independent sequencing experiments, *P* values were calculated using Wald test with Benjamini–Hochberg correction. **e**–**g** Cumulative distributions of ribosome density change (**e**), mRNA change (**f**), and relative ribosome density change (TE) (**g**) for codon-rich, codon-poor, and total transcripts. All the genes were divided into codon-rich genes (top 20%) and codon-poor genes (bottom 20%) based on the content of 5A-ending codons (including AAA, CAA, GAA, AGA, and GGA). 2 independent sequencing experiments, Two-sided Mann–Whitney test. **h**–**j** Cumulative distributions of ribosome density change (**h**), mRNA change (**i**), and relative ribosome density change (**j**) for codon-rich, codon-poor, and total transcripts. All the genes were divided into codon-rich genes (top 20%) and codon-poor genes (bottom 20%) based on the content of 5G-ending codons (including AAG, CAG, GAG, AGG, and GGG). 2 independent sequencing experiments, Two-sided Mann–Whitney test. Source data are provided as a Source Data file.

https://doi.org/10.1038/s41467-025-64144-0

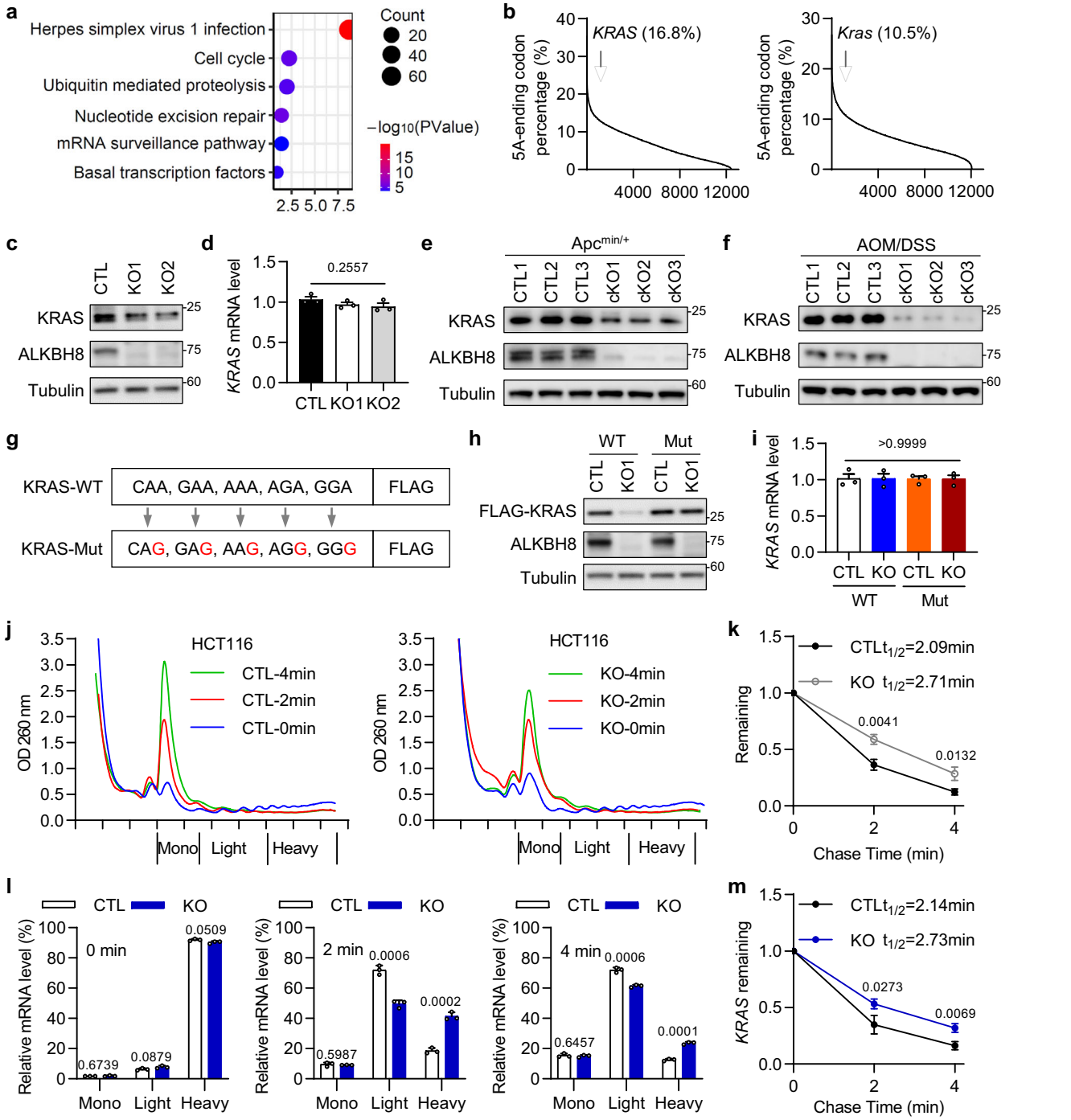

Fig. 5 | ALKBH8 regulates the translation elongation of KRAS. a KEGG analysis of genes enriched with A-ending codons and exhibiting increased ribosome density following ALKBH8 knockout. 2 independent sequencing experiments, *P* values were calculated using DAVID (modified Fisher's exact test with Benjamini–Hochberg correction). **b** Transcriptomic distribution of the percentage of 5A-ending codons. The percentage of A-ending codons for *KRAS* and *Kras* gene was highlighted. **c** Immunoblot analysis of KRAS expression in CTL and A8-KO HCT116 cells. **d** *KRAS* mRNA levels in control, A8-KO HCT116 cells. Mean ± SEM, 3 biological replicates, one-way ANOVA with Tukey's multiple comparisons test. **e** Immunoblot analysis of 3 pairs of tumors from *Apc*$^{min/+}$;*Alkbh8*^{CTL} and *Apc*$^{min/+}$;*Alkbh8*^{cKO} mice. **f** Immunoblot analysis of 3 pairs of tumors from *Alkbh8*^{CTL} and *Alkbh8*^{cKO} mice of AOM/DSS induction. **g** Schematic of synonymous mutation of *KRAS* gene. **h** The expression of wild-type *KRAS* gene and its synonymous mutant in CTL and A8-KO cells. **i** The mRNA level of KRAS in CTL and A8-KO HCT116 cells. Mean ± SEM, 3 biological replicates, one-way ANOVA with Tukey's multiple comparisons test. **j** Ribosomal elongation speed was measured using harringtonine chase. Polysome profiles of CTL cells or A8-KO cells treated with harringtonine (2 ug/mL) for indicated times. Monosome (80S) and polysomes were highlighted and the P/M ratio change was quantified in the right panel. **k** The polysome dissociation halftime in (**g**) was calculated. Mean ± SEM, 3 biological replicates, two-sided *t*-test. **l** The distributions of *KRAS*/*ACTB* mRNAs in the polysome fractions of (**g**). Mean ± SEM, 3 biological replicates, two-sided *t*-test. **m** The dissociation halftime of *KRAS* mRNA in (**i**) was calculated. Mean ± SEM, 3 biological replicates, two-sided *t*-test. Source data are provided as a Source Data file.

https://doi.org/10.1038/s41467-025-64144-0

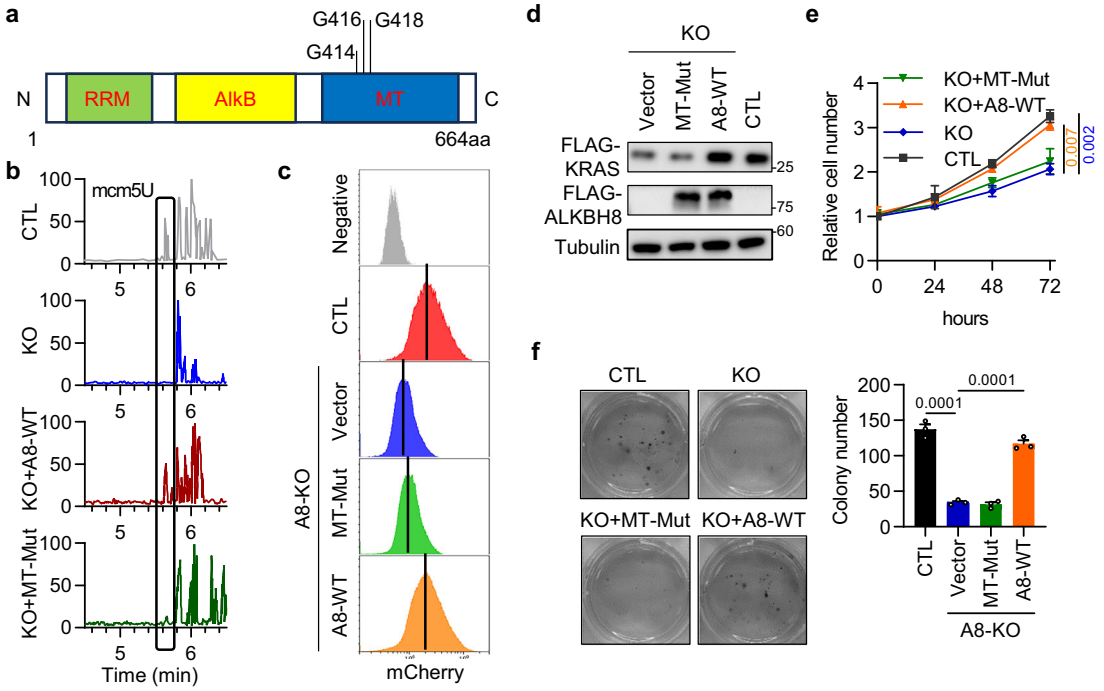

Fig. 6 | The methyltransferase domain is required for ALKBH8-regulated translation. a Schematic of ALKBH8 domain structure and its key amino acids. **b** Mass spectrometry analysis of cm5U, mcm5U, and mcm5s2U levels in tRNAs from CTL and A8-KO HCT116 cells, 3 biological replicates. **c** OP-Puro labeling analysis of global translation levels, 3 biological replicates. **d** Immunoblot analysis of CTL cells, A8-KO cells reconstituted with wild-type A8 or MT-mutant. **e** Proliferation analysis of CTL cells, A8-KO cells reconstituted with wild-type A8 or MT-mutant. Mean ± SEM, 3 biological replicates, one-way ANOVA with Tukey's multiple comparisons test. **f** Colony formation assay of CTL cells, A8-KO cells reconstituted with wild-type A8 or MT-mutant. Mean ± SEM, 3 biological replicates, one-way ANOVA with Tukey's multiple comparisons test. Source data are provided as a Source Data file.

Discussion

Dysregulated gene expression at either the transcriptional or translational level contributes to intestinal tumorigenesis. In the present study, we showed that U34-modifying enzyme ALKBH8, which catalyzes the mcm5-U34 tRNA modifications and the derivatives, is upregulated in human CRC samples, as well as in mouse intestinal tumors. The genetic ablation of *Alkbh8* slightly affects intestinal homeostasis but dramatically reduces tumor formation in mice and affects colorectal cancer cell viability in vitro. Ribosome profiling data demonstrated that a group of mRNAs enriched in A-ending codons requires ALKBH8 for their translational elongation. In particular, ALKBH8 regulates KRAS expression to promote cell cycle transition. Therefore, our results highlight the importance of ALKBH8 in remodeling gene expression by regulating translation elongation during intestinal tumorigenesis.

Studies have shown that the function of ALKBH8 is context- and tissue-dependent. Yeast Trm8, the analogue of human ALKBH8, is not required under normal conditions, while essential for DNA damage response[20]. Depletion of *Alkbh8* gene in mice mainly induces dysfunction of the central nervous system[36]. Moreover, mice lacking ALKBH8 show no obvious lung defects but are more sensitive to naphthalene-induced lung injury[37]. Consistent with these reports, our study showed that ALKBH8 is dispensable for normal intestinal homeostasis while essential for tumorigenesis. ALKBH8 is upregulated in CRC and its overexpression directly promotes CRC development. The cancer specificity of ALKBH8 depends on its expression level: it is weakly expressed in normal intestinal epithelia but upregulated in cancer cells, driven by the activated Wnt/β-catenin signaling. Thus, ALKBH8-regulated gene expression may represent an attractive convergent mechanism to which cancer cells become addicted during intestinal tumorigenesis.

Here, we provided evidence that ALKBH8 regulates mRNA translation elongation in CRC cells. Depletion of ALKBH8 in CRC cells induces ribosomal pausing at codons AAA, CAA, GAA, AGA, and GGA, leading to increased ribosome density at the transcripts enriched with these codons. This likely results from inefficient decoding, since loss of ALKBH8 impairs the translation elongation speed. The rescuing experiments demonstrated that the methyltransferase domain is required for ALKBH8-regulated mRNA translation, highlighting the importance of ALKBH8-mediated mcm5U modification for decoding efficiency. Other studies, along with ours, indicate that U34 modifications play a complex role in regulating mRNA translation and the U34 enzymes affect the biased usage of different codons. Yeast strains lacking ELP homologs induce ribosome accumulations at AAA, CAA, and GAA codons[15,38,39], but deletion of ALKBH8 homolog Trm8 in yeast mainly impairs expression of genes enriched with AGA and GAA codons[20,21]. These differential effects may be influenced by the complex enzymatic cascade in catalyzing U34 modifications. Although ALKBH8 and ELPs work cooperatively to catalyze the formation of mcm5U, the mcm5U could be further catalyzed by CTUs to form mcm5s2U. Moreover, the AlkB domain of ALKBH8 could catalyze hydroxylation of mcm5U to form mchm5U, which is specific to ALKBH8[17,18]. How these derivatives of mcm5U participate in the regulation of decoding process warrants further investigation.

Although both ELP3 and ALKBH8 participate in the wobble uridine tRNA modification pathway, the intestinal phenotypes resulting from their inactivation are markedly different, particularly with respect to tuft cell differentiation. *Elp3* deficiency selectively impairs the development of Dclk1$^+$ tuft cells without significantly affecting other epithelial lineages[22]. In contrast, *Alkbh8* knockout increases secretory cell lineages, including Dclk1$^+$ tuft cells and Muc2$^+$ goblet cells, while downregulating stem cell markers such as Lgr5 and Ki67, indicating that ALKBH8 is essential for maintaining intestinal stemness. These opposite effects on tuft cells suggest distinct regulatory roles, which may arise from the different functions of cm5U and mcm5U modifications on specific tRNAs and their differential decoding properties,

https://doi.org/10.1038/s41467-025-64144-0

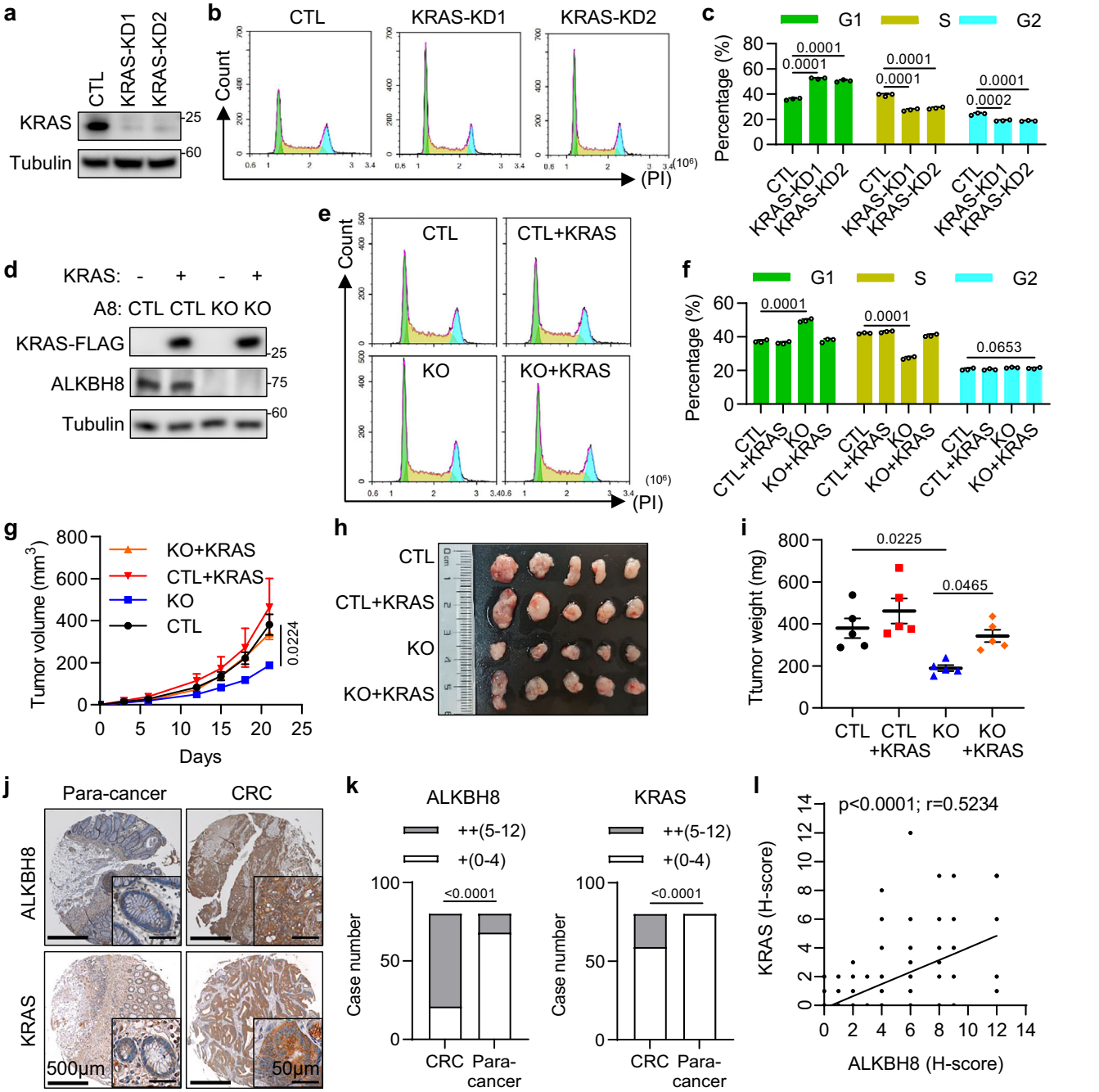

Fig. 7 | KRAS contributes to ALKBH8-mediated CRC progression. **a** Immunoblotting analysis of control cells and KRAS knockdown cells. **b** Cell cycle analysis of control cells and KRAS knockdown cells. **c** Statistical analysis of cell cycle distribution in (**b**). Mean ± SEM, 3 biological replicates, one-way ANOVA with Dunnett's multiple comparisons test. **d** Immunoblotting analysis of control cells and A8-KO cells with or without KRAS overexpression. **e** Cell cycle analysis of control cells and A8-KO cells with or without KRAS overexpression. **f** Statistical analysis of cell cycle distribution in (**e**). Mean ± SEM, 3 biological replicates, one-way ANOVA with Tukey's multiple comparisons test. **g** The volume of xenograft tumors from mice implanted with control cells and A8-KO cells with or without KRAS expression. Mean ± SEM. 5 mice for each group, one-way ANOVA with Tukey's multiple comparisons test. **h** The images of xenograft tumors from mice implanted with control cells and A8-KO cells with or without KRAS expression. **i** The analysis of tumor weight in (**h**). Mean ± SEM, 5 mice for each group, one-way ANOVA with Tukey's multiple comparisons test. **j** Representative immunohistochemistry (IHC) images depicting KRAS protein level and ALKBH8 protein level in adjacent normal tissue and CRC tissue in a CRC tissue array. **k** IHC scoring of ALKBH8 and KRAS in para-cancer tissues and CRC tissues. Distribution of low (+) and high (++) levels of ALKBH8 and KRAS protein expression in para-cancer tissues and CRC tissues. Two-sided Chi-square test; n = 80 for each group. **l** Two-sided Pearson's correlation showed relationship of ALKBH8 and KRAS by using H-score. n = 80. Source data are provided as a Source Data file.

ultimately leading to distinct sets of target transcripts. Mechanistically, ELP3 maintains Dclk1$^+$ cells by promoting SOX9 translation, whereas ALKBH8 promotes crypt cell proliferation by enhancing KRAS translation.

KRAS is the most frequently mutated oncogene in human cancers[40]. In addition to the activating mutations, the overexpression of RAS proteins also contributes to its oncogenic activity in a variety of human cancers including colorectal cancer. KRAS translation has several distinctive features. First, the 5′-UTR of KRAS mRNA harbors rG4 structures, which act as repressors of translation initiation[41]. RNA helicases, such as eIF4A, are required to unwind the rG4s and rescue KRAS translation[42]. Second, the KRAS gene is enriched for rare codons,

leading to reduced translation and expression[43]. Our results showed that the KRAS gene is enriched with A-ending codons, and its translation requires ALKBH8-mediated tRNA methylation. We also establish a functional link between KRAS and ALKBH8 in CRC progression as KRAS depletion impairs cell growth while KRAS re-expression rescues cell growth defects in ALKBH8-KO cells. Remarkably, the expression of ALKBH8 and KRAS was significantly correlated in CRC samples. These findings demonstrate that ALKBH8-mediated U34 tRNA modification is critical for KRAS expression to support colorectal tumorigenesis. Although significant progress has been made with directly targeted drugs for KRAS (G12C) mutations, effective inhibitors for other KRAS mutations remain elusive. Indirect targeting of KRAS mutation, such as by modulating KRAS expression, upstream regulators, or downstream effectors, has been considered an alternative anti-RAS strategy[40]. The requirement of ALKBH8 in translating A-ending codons of the KRAS gene offers a possible strategy in the development of pan-KRAS inhibitors.

In summary, our findings highlighted an essential role of ALKBH8 in CRC progression, with potential implications for cancer intervention. In addition, our results established a model for ALKBH8-mediated and tRNA modification-dependent translational regulation, which may guide the understanding of the development of other disorders associated with ALKBH8 dysregulation.

Methods

Ethics statement

All animal studies complied with the Guide for the Care and Use of Laboratory Animals by the Medical Experimental Animal Care Commission of Zhejiang University. All animal studies used the protocol approved by the Medical Experimental Animal Care Commission of Zhejiang University (ZJU20240214). According to the approved protocol, the maximal tumor size permitted was 15 mm in diameter. We confirm that this limit was not exceeded in any of the experiments described in this study.

Mice were inspected daily for changes in body weight, behavior, and overall health status. Disease progression was assessed on the basis of weight reduction, stool abnormalities, and rectal bleeding. Experimental endpoints were either predetermined time points or humane criteria, which included >20% loss of baseline body weight, severe diarrhea, rectal prolapse, ulceration, respiratory distress, or inability to feed or drink. Animals reaching these endpoints were euthanized promptly according to institutional animal welfare guidelines.

Mice used for in vivo experiments

All mice were bred and maintained under specific pathogen-free conditions in the Laboratory Animal Center of Zhejiang University. Housing was carried out with controlled environmental parameters, including a 12-h light/dark schedule, regulated temperature (approximately 22 °C), and 50–60% relative humidity. Standard chow and water were available without restriction.

A global *Alkbh8* knockout line on the C57BL/6 background was generated by Cyagen Biosciences (China) through deletion of exons 2-5. A conditional *Alkbh8* knockout line (*Alkbh8*$^{F/F}$), which carries LoxP sites flanking exons 3–6, and the Villin-Cre strain were both produced by GemPharmatech (China) on a C57BL/6 background. *Apc*$^{F/F}$, *Apc*$^{min/+}$, and *Lgr5-EGFP-IRES-creERT2* strains were obtained from the Jackson Laboratory. To establish *Alkbh8* intestinal epithelial-specific knockout mice (*Alkbh8*^{cKO}), *Alkbh8*$^{F/F}$ mice were crossed with *Villin-Cre* mice.

Apc$^{min/+}$ spontaneous mouse tumor model

To assess tumorigenesis driven by *Apc* mutation, *Alkbh8*$^{F/F}$, *Alkbh8*^{KO}, and *Alkbh8*^{cKO} mice carrying one mutant *Apc* allele (*Apc*$^{min/+}$) were aged for six months to allow spontaneous tumor development. At the end of this period, mice were euthanized, and tumors and surrounding tissues were collected for analysis.

The AOM/DSS-induced mouse tumor model

Male *Alkbh8*^{CTL} and *Alkbh8*^{cKO} littermates at 8 weeks of age received a single intraperitoneal injection of azoxymethane (AOM, Sigma) at a dose of 10 mg/kg body weight. Beginning one week later, animals were exposed to three cycles of dextran sulfate sodium (DSS, MP Biomedicals) treatment, each cycle consisting of 7 consecutive days of 2.5% (w/v) DSS in drinking water followed by a 14-day recovery period on regular water. At week 12, mice were euthanized, and colons were harvested for assessment of tumor incidence, number, and size.

The DSS-induced colitis model

Male *Alkbh8*^{CTL} and *Alkbh8*^{cKO} littermates at 8 weeks of age were given 2.5% (w/v) DSS in drinking water for 7 consecutive days beginning on day 1, while control mice received untreated water. On day 9, animals were euthanized, and colons were excised for measurements of length and subsequent histological analyses. Histological scores were determined using a scale based on the severity of inflammation (0-3), ulceration (0-3)[44].

Xenograft mouse model

1×10^6 HCT116 cells were resuspended in 100 µL sterile PBS and injected subcutaneously into the right flank of 6-week-old male mice. Tumor growth and body weight were monitored every 2-3 days using calipers to measure tumor length (L) and width (W), with tumor volume calculated using the formula: $V = (L \times W^2)/2$. Mice were sacrificed 21 days post-injection, and tumors were excised, weighed, and collected for further histological analysis.

Crypt isolation, culture, and treatment

Small intestinal crypts were isolated from normal or adenomatous intestinal tissues using EDTA-based dissociation. The tissues were cut into small fragments and washed with cold PBS until the supernatant was clear. The fragments were then incubated in 10 mM EDTA on ice for 30 minutes, followed by vigorous shaking to release crypts. The crypt suspension was filtered through a 70 µm cell strainer and collected by centrifugation. Crypts were embedded in Matrigel (356231, Corning) and seeded into 24-well plates. After polymerization, wells were overlaid with Organoid Growth Medium (06005, STEMCELL) and maintained at 37 °C in a humidified incubator with 5% CO_2. The medium was changed every 2–3 days. Organoid formation and growth were monitored using light microscopy.

Organoids were collected and digested from Matrigel using cold PBS, incubated with lentivirus in suspension, and centrifuged briefly. After overnight infection, organoids were embedded in fresh Matrigel and cultured in Organoid Growth Medium.

Human colorectal cancer tissue samples

Commercial colorectal cancer tissue microarrays (catalog numbers OD-CT-DgCol01-006 and HcolA030PG06) were obtained from Shanghai Outdo Biotech Company. The study was approved by the company's institutional ethics review board, and written informed consent was secured from all participants. All procedures complied with the ethical standards outlined in the Declaration of Helsinki and the Belmont Report of the Department of Health and Human Services.

Histology and immunohistochemistry

After removal, intestinal tissues were rinsed in DPBS, fixed in 10% neutral buffered formalin, and processed for paraffin embedding. Paraffin blocks were sectioned at 5 µm thickness and stained with hematoxylin and eosin (H&E) for histological examination.

For immunohistochemistry, sections were first deparaffinized, rehydrated, and subjected to heat-mediated antigen retrieval in 0.01 M citrate buffer (pH 6.0) using a microwave oven. Endogenous peroxidase activity was blocked with 3% hydrogen peroxide, and nonspecific binding was minimized by incubation with 5% goat serum. Slides were incubated overnight at 4 °C with primary antibodies, followed by horseradish peroxidase (HRP)-conjugated secondary antibodies. Signals were visualized using diaminobenzidine (DAB) and counterstained with hematoxylin. Finally, images were acquired by digital scanning with an Olympus VS200 slide scanner.

Immunohistochemical staining of colorectal cancer tissue arrays for KRAS and ALKBH8 was evaluated using a semi-quantitative four-point scale, ranging from 0 (no detectable staining) to 3 (strong membranous and cytoplasmic staining). The staining intensity was then multiplied by the proportion of positive tumor cells (graded 0–4), yielding a composite H-score with a maximum value of 12.

Antibodies used in the experiments: ALKBH8 (1/50 dilution, TA365348, Origene), KRAS (1/500 dilution, 16155-1-AP, Proteintech), Brdu (10 μg/mL, ab1893, Abcam), Ki67 (1/200 dilution, ab16667, Abcam), β-catenin (1/100 dilution, A2064, Abclonal).

Immunofluorescence staining

Intestinal paraffin sections (5 μm) were deparaffinized, rehydrated, and subjected to heat-mediated antigen retrieval in 0.01 M citrate buffer (pH 6.0). After blocking with 5% goat serum in PBST, slides were incubated overnight at 4 °C with primary antibodies and then with fluorophore-conjugated secondary antibodies. Nuclei were counterstained with DAPI, mounted in antifade medium, and examined using a confocal microscope.

Primary antibodies used: ALKBH8 (1/50 dilution, TA365348, Origene), Ki67 (1/250 dilution, ab16667, Abcam), MUC2 (1/200 dilution, 27675-1-AP, Proteintech), DCLK1 (1/200 dilution, 21699-1-AP, Proteintech), LYZ (1/200 dilution, 15013-1-AP, Proteintech), CD68 (1/200 dilution, 28058-1-AP, Proteintech), CD86 (1/200 dilution, 13395-1-AP, Proteintech), CD163 (1/200 dilution, 16646-1-AP, Proteintech), Olfm4 (1/200 dilution, 39141, CST).

Cell culture and treatments

HCT116 (CCL-247), RKO (CRL-2577), and HEK293T (CRL-3216) cells were purchased from ATCC. Cells cultured in DMEM medium (C11995500BT, Gibco) supplemented with 10% fetal bovine serum (B118-500, Nobimpex). Cells were maintained at 37 °C in an atmosphere containing 5% CO_2.

Generation of ALKBH8 knockout cell lines

To achieve *ALKBH8* ablation, sgRNA targeting human *ALKBH8* was subcloned into the vector pLenti-U6-gRNA-Cas9 (D8309, Beyotime) at the BsmBI site. HCT116 and RKO cells were transfected with the construct using Lipofectamine 2000 transfection reagent (11668019, ThermoFisher Scientific), followed by selection with 1 μg/mL puromycin (ST551, Beyotime) for 5 days.

Generation of knockdown and overexpression cell line

Cells were transduced with lentiviruses to achieve either stable knockdown or overexpression. We generated lentiviruses by transfection of the pLKO.1 or pCDH constructs described above, together with psPAX2 and pMD2.G into 293 T cells using Lipofectamine 2000 Reagent. The resulting viruses were used to infect the HCT116 and RKO cells. Stably transduced cells were selected with puromycin.

Immunoblotting

Cells were lysed in RIPA buffer (P0013, Beyotime) supplemented with protease inhibitors, and lysates were clarified by centrifugation. Protein concentrations were determined using a BCA assay, and equal amounts of protein were resolved by SDS–PAGE before being transferred onto PVDF membranes (IPVH00010, Millipore). After blocking with 5% bovine serum albumin in TBST, membranes were incubated overnight at 4 °C with the indicated primary antibodies, followed by incubation with HRP-conjugated secondary antibodies. Protein bands were visualized using an enhanced chemiluminescence detection system (Amersham Imager).

Antibodies used in the experiments: ALKBH8 (1/1000 dilution, TA365348, Origene), β-catenin (1/1000 dilution, A2064, Abclonal), c-MYC (1/2000 dilution, 10828-1-AP, Proteintech), GAPDH (1/10000 dilution, AC002, Abclonal), β-Actin (1/100000 dilution, AC026, Abclonal), α-tubulin (1/2000 dilution, A6830, Abclonal), Puromycin (1/1000 dilution, EQ0001, Kerafast), KRAS (1/1000 dilution, 16155-1-AP, Proteintech), FLAG (1/1000 dilution, F1804, Sigma), CDK1 (1/2000 dilution, 19532−1-AP, Proteintech), LGR5 (1/1000 dilution, 30007−1-AP, Proteintech), CTU1 (1/1000 dilution, 31537−1-AP, Proteintech), ELP3 (1/1000 dilution, 17016−1-AP, Proteintech).

Quantitative RT-PCR

Total RNA was isolated from tissues or cells using TRIzol reagent (15596026, Invitrogen). 1μg of total RNA sample was reverse transcribed with the Evo M-MLV RT Premix (AG11706, Accurate Biology). Real-time PCR was performed using the SYBR Green Pro Taq HS Premix (AG11701, Accurate Biology) on a LightCycler 480 real-time PCR system (Roche). Relative gene expression was normalized to the expression of ACTB or GAPDH and was calculated using the $2^{(-\Delta\Delta CT)}$ method. The PCR primers were synthesized by Tsingke Biotechnology (China) and listed in Data S4.

Luciferase Reporter Assay

Cells were seeded in a 12-well plate at a density of 2×10^5 cells per well and transfected with the firefly luciferase reporter plasmid along with the Renilla luciferase control plasmid. After 24 hours of transfection, cells were lysed, and luciferase activity was measured using the Dual-Luciferase Assay System (E1910, Promega). The firefly luciferase activity was normalized to Renilla luciferase.

LC-MS/MS analysis

Total RNA was isolated from tissues or cells using TRIzol reagent. The total RNA was separated on a 15% TBE-Urea gel (EC6885BOX, Invitrogen), and tRNA was extracted from the gel corresponding to the size of 70-90 nucleotides. 200 ng of tRNA was digested by nuclease P1 (2 U) at 42 °C for 2 h, followed by the addition of NH4HCO3 (1 M, 3 μL) and alkaline phosphatase (0.5 U) and incubation at 37 °C for 2 h. The nucleosides were separated by reverse-phase ultra-performance liquid chromatography on a C18 column with online mass spectrometry detection using Agilent 6410 QQQ triple-quadrupole LC mass spectrometer in positive electrospray ionization mode. The nucleosides were quantified using the nucleoside to base ion mass transitions of 317.31 to 185.21 (mcm5U), 303.2 to 171.1 (cm5U), and 333.2 to 169.1 (mcm5s2U). Quantification was performed in comparison with standard mcm5U (NM45525, Biosynth), cm5U (NC159474, Biosynth), and mcm5s2U (NM159492, Biosynth) from the same batch of samples.

Plasmids construction

The coding regions of wild-type and mutant forms of ALKBH8 with a FLAG tag were cloned into the vector pCDH-CMV-MCS-EF1-Puro at the XbaI site. The coding regions of wild-type and mutant forms of KRAS with a FLAG tag were cloned into the same vector at the NheI/NotI sites. Cloning was performed using ClonExpress II One Step Cloning Kit (C112-01, Vazyme). For shRNA knockdown experiments, specific shRNA oligos were annealed and cloned into the lentiviral vector pLKO.1. For luciferase experiments, wild-type and mutant forms of ALKBH8 promoter were cloned into the vector pGL3-Enhancer at the HindIII site. The specific primers were synthesized by Tsingke Biotechnology (China) and listed in Data S4.

Cell proliferation assay

For the CCK-8 assay, cells were seeded at 5×10^3 cells per well in a 96-well plate and allowed to adhere for 12 hours. At specific time points, 10 μL of CCK-8 reagent (CK04, Dojindo Laboratory) was added to each well and incubated for 1.5 hours. Absorbance at 450 nm was measured using a microplate reader.

For the soft agar colony formation assay, a 0.5% agarose bottom layer was prepared in a 6-well plate, and 2000 cells mixed with 0.3% agarose were overlaid in each well. The plates were incubated for 2-3 weeks, with medium added every 2-3 days. Colonies were stained with 1 mg/mL nitroblue tetrazolium (ST362, Beyotime) overnight. Colonies were then imaged and counted using ImageJ software.

Cell cycle assay

Cells were seeded at a density of 5×10^5 cells per 6-well plate and allowed to adhere overnight. After treatment or incubation for the desired time, cells were harvested and fixed in 70% ethanol at 4 °C overnight. Cells were then washed with PBS and stained with propidium iodide (PI) solution for 30 minutes at 37 °C in the dark. Cell cycle distribution was analyzed using an ACEA NovoCyteTM flow cytometer, and data were processed with the accompanying software to determine the proportions of cells in G1, S, and G2 phases.

O-propargyl-puromycin labeling and flow cytometry

Cells were incubated with O-propargyl-puromycin (OP-Puro, C10457, Invitrogen) for 30 minutes at 37 °C to allow incorporation into nascent polypeptide chains. After labeling, cells were harvested, fixed with 4% paraformaldehyde for 15 minutes at room temperature, and permeabilized using 0.5% Triton X-100. The incorporated OP-Puro was detected using a click reaction with 594 picolyl azide according to the manufacturer's instructions. The fluorescent signal (mCherry channel) was analyzed by flow cytometry to assess global protein synthesis activity.

Polysome profiling

For ribosome chase experiments, cells were first exposed to harringtonine (HHT, 2 μg/mL; HY-N0862, MedChemExpress) for 0, 2.5, or 5 min, and subsequently treated with cycloheximide (CHX, 100 μg/mL; HY-12320, MedChemExpress) for 3 min to stabilize ribosomes on mRNA. After harvesting, cell pellets were lysed on ice in polysome lysis buffer (10 mM HEPES, pH 7.4, 5 mM $MgCl_2$, 100 μg/mL CHX, 100 mM KCl, 5 mM DTT, and 1% Triton X-100). Lysates were clarified by centrifugation, and the resulting supernatants were layered onto linear 10–50% (w/v) sucrose gradients prepared in polysome buffer (10 mM HEPES, pH 7.4, 5 mM $MgCl_2$, 100 mM KCl, 100 μg/mL CHX). Gradients were ultracentrifuged at 178,305 × *g* for 2.5 h at 4 °C using a Beckman SW41Ti rotor. Fractionation was performed with a BioComp Gradient Station equipped with UV detection and collected via a Gilson FC203B fraction collector. RNA from individual fractions was extracted with TRIzol reagent and used for RT–qPCR analysis.

RNA-seq

Total RNA was extracted with TRIzol reagent, and poly(A)$^+$ RNA was purified using Dynabeads Oligo$(dT)_{25}$ (61005, Invitrogen). The enriched mRNA was then fragmented to an average size of 100 ~ 200 nucleotides with the RNA Fragmentation Reagents (AM8740, Ambion), followed by library preparation and high-throughput sequencing.

Ribo-seq

Cells were collected in polysome lysis buffer, and cell lysates were clarified by centrifugation at 12,000 × *g* for 10 min at 4 °C. The resulting supernatants were incubated with RNase I (AM2295, Ambion) for 1 h at 4 °C to digest unprotected RNA. Ribosome-protected fragments (RPFs) were subsequently pelleted through a 1 M sucrose cushion by ultracentrifugation at 449,165 × *g* for 134 min using an MLA150 rotor (Beckman). Total RNA was recovered with TRIzol reagent, and the ends of the protected fragments were phosphorylated using T4 polynucleotide kinase (T4 PNK; B0201S, NEB). Sequencing libraries were generated with the Small RNA Library Prep Set for Illumina (E7330S, NEB) following the manufacturer's instructions.

Single-cell RNA sequencing of mouse colorectal tumors

Colorectal tumors were collected from AOM/DSS-treated mice and enzymatically digested into a single-cell suspension. scRNA-seq libraries were prepared using the DNBelab C Series High-throughput Single-Cell RNA Library Preparation Set (940-001818-00, MGI) following the manufacturer's instructions. Libraries were sequenced on the DNBSEQ platform with paired-end reads.

Sequencing data analysis

Adaptor sequences and low-quality bases were removed from raw reads using Cutadapt (v3.7). Reads shorter than 15 nt after trimming were discarded. The cleaned reads were aligned to the genome with HISAT2 (v2.1.0), allowing up to two mismatches. For Ribo-seq, only footprints mapped to CDS were considered for quantifying translation, and expression levels were calculated as RPKM. For RNA-seq, expression was determined from reads mapped to full transcripts, also in RPKM units. Translational efficiency (TE) was assessed as the ratio of ribosome profiling signal (Ribo-seq FPKM) to transcript abundance (RNA-seq FPKM).

For single-cell RNA-seq, Raw data were processed with DNBC4tools (v2.1.0) and downstream analysis using the Seura R package (v5.0). Cells with fewer than 200 or more than 6000 expressed genes, or with >15% mitochondrial gene content, were excluded. Doublets were removed using DoubletFinder (v2.0.4). Batch correction was performed with Harmony, followed by clustering, dimensionality reduction (PCA, UMAP), and differential expression analysis.

Statistics and Reproducibility

Statistical analysis was performed using GraphPad Prism 9 software (GraphPad Software, Inc.). *P* values were calculated using the two-sided t-test or one-way ANOVA unless stated otherwise. Representative blots and images shown in the figures were obtained from at least three independent experiments. The sample size was determined based on prior studies and the complexity of the assay. No data were excluded from the analyses. The experiments were randomized, and investigators were blinded to allocation during experiments and outcome assessment.

Reporting summary

Further information on research design is available in the Nature Portfolio Reporting Summary linked to this article.

Data availability

The RNA-seq, Ribo-seq, and single-cell RNA-seq data generated in this study have been deposited in the Gene Expression Omnibus (GEO) database under accession code GSE278268 and are publicly available. Source data are provided with this paper.

References

1. Lao, V. V. & Grady, W. M. Epigenetics and colorectal cancer. *Nat. Rev. Gastroenterol. Hepatol.* **8**, 686–700 (2011).
2. Fearon, E. R. Molecular genetics of colorectal cancer. *Annu Rev. Pathol.* **6**, 479–507 (2011).
3. Fearon, E. R. & Vogelstein, B. A genetic model for colorectal tumorigenesis. *Cell* **61**, 759–767 (1990).
4. Nusse, R. & Clevers, H. Wnt/beta-catenin signaling, disease, and emerging therapeutic modalities. *Cell* **169**, 985–999 (2017).

5. Morin, P. J., Kinzler, K. W. & Sparks, A. B. beta-catenin mutations: Insights into the APC Pathway and the power of genetics. *Cancer Res* **76**, 5587–5589 (2016).
6. Vogelstein, B. et al. Genetic alterations during colorectal-tumor development. *N. Engl. J. Med* **319**, 525–532 (1988).
7. Faller, W. J. et al. mTORC1-mediated translational elongation limits intestinal tumour initiation and growth. *Nature* **517**, 497–500 (2015).
8. Han, B. et al. YTHDF1-mediated translation amplifies Wnt-driven intestinal stemness. *EMBO Rep.* **21**, e49229 (2020).
9. Tang, J. et al. The IGF2BP3-COPS7B Axis Facilitates mRNA Translation to Drive Colorectal Cancer Progression. *Cancer Res* **83**, 3593–3610 (2023).
10. Roundtree, I. A., Evans, M. E., Pan, T. & He, C. Dynamic RNA Modifications in Gene Expression Regulation. *Cell* **169**, 1187–1200 (2017).
11. Agris, P. F. Bringing order to translation: the contributions of transfer RNA anticodon-domain modifications. *EMBO Rep.* **9**, 629–635 (2008).
12. Kalhor, H. R. & Clarke, S. Novel methyltransferase for modified uridine residues at the wobble position of tRNA. *Mol. Cell Biol.* **23**, 9283–9292 (2003).
13. Huang, B., Lu, J. & Bystrom, A. S. A genome-wide screen identifies genes required for formation of the wobble nucleoside 5-methoxycarbonylmethyl-2-thiouridine in saccharomyces cerevisiae. *RNA* **14**, 2183–2194 (2008).
14. Noma, A., Sakaguchi, Y. & Suzuki, T. Mechanistic characterization of the sulfur-relay system for eukaryotic 2-thiouridine biogenesis at tRNA wobble positions. *Nucleic Acids Res* **37**, 1335–1352 (2009).
15. Rezgui, V. A. et al. tRNA tKUUU, tQUUG, and tEUUC wobble position modifications fine-tune protein translation by promoting ribosome A-site binding. *Proc. Natl Acad. Sci. USA* **110**, 12289–12294 (2013).
16. Rapino, F. et al. Codon-specific translation reprogramming promotes resistance to targeted therapy. *Nature* **558**, 605–609 (2018).
17. Fu, Y. et al. The AlkB domain of mammalian ABH8 catalyzes hydroxylation of 5-methoxycarbonylmethyluridine at the wobble position of tRNA. *Angew. Chem. Int Ed. Engl.* **49**, 8885–8888 (2010).
18. van den Born, E. et al. ALKBH8-mediated formation of a novel diastereomeric pair of wobble nucleosides in mammalian tRNA. *Nat. Commun.* **2**, 172 (2011).
19. Songe-Moller, L. et al. Mammalian ALKBH8 possesses tRNA methyltransferase activity required for the biogenesis of multiple wobble uridine modifications implicated in translational decoding. *Mol. Cell Biol.* **30**, 1814–1827 (2010).
20. Begley, U. et al. Trm9-catalyzed tRNA modifications link translation to the DNA damage response. *Mol. Cell* **28**, 860–870 (2007).
21. Deng, W. et al. Trm9-Catalyzed tRNA modifications regulate global protein expression by codon-biased translation. *PLoS Genet* **11**, e1005706 (2015).
22. Ladang, A. et al. Elp3 drives Wnt-dependent tumor initiation and regeneration in the intestine. *J. Exp. Med* **212**, 2057–2075 (2015).
23. Delaunay, S. et al. Elp3 links tRNA modification to IRES-dependent translation of LEF1 to sustain metastasis in breast cancer. *J. Exp. Med* **213**, 2503–2523 (2016).
24. Chen, D. et al. Elp3-mediated codon-dependent translation promotes mTORC2 activation and regulates macrophage polarization. *EMBO J.* **41**, e109353 (2022).
25. Waszak, S. M. et al. Germline elongator mutations in sonic hedgehog medulloblastoma. *Nature* **580**, 396–401 (2020).
26. Shimada, K. et al. A novel human AlkB homologue, ALKBH8, contributes to human bladder cancer progression. *Cancer Res* **69**, 3157–3164 (2009).
27. Ohshio, I. et al. ALKBH8 promotes bladder cancer growth and progression through regulating the expression of survivin. *Biochem Biophys. Res Commun.* **477**, 413–418 (2016).
28. Morin, P. J. et al. Activation of beta-catenin-Tcf signaling in colon cancer by mutations in beta-catenin or APC. *Science* **275**, 1787–1790 (1997).
29. Bottomly, D., Kyler, S. L., McWeeney, S. K. & Yochum, G. S. Identification of {beta}-catenin binding regions in colon cancer cells using ChIP-Seq. *Nucleic Acids Res* **38**, 5735–5745 (2010).
30. Korinek, V. et al. Constitutive transcriptional activation by a beta-catenin-Tcf complex in APC-/- colon carcinoma. *Science* **275**, 1784–1787 (1997).
31. Chen, J. & Huang, X. F. The signal pathways in azoxymethane-induced colon cancer and preventive implications. *Cancer Biol. Ther.* **8**, 1313–1317 (2009).
32. Ingolia, N. T., Lareau, L. F. & Weissman, J. S. Ribosome profiling of mouse embryonic stem cells reveals the complexity and dynamics of mammalian proteomes. *Cell* **147**, 789–802 (2011).
33. Gao, X. et al. Quantitative profiling of initiating ribosomes in vivo. *Nat. Methods* **12**, 147–153 (2015).
34. Kim, D., Xue, J. Y. & Lito, P. Targeting KRAS(G12C): From inhibitory mechanism to modulation of antitumor effects in patients. *Cell* **183**, 850–859 (2020).
35. Peeper, D. S. et al. Ras signalling linked to the cell-cycle machinery by the retinoblastoma protein. *Nature* **386**, 177–181 (1997).
36. Honda, K. et al. ALKBH8 contributes to neurological function through oxidative stress regulation. *PNAS Nexus* **3**, pgae115 (2024).
37. Leonardi, A. et al. The epitranscriptomic writer ALKBH8 drives tolerance and protects mouse lungs from the environmental pollutant naphthalene. *Epigenetics* **15**, 1121–1138 (2020).
38. Zinshteyn, B. & Gilbert, W. V. Loss of a conserved tRNA anticodon modification perturbs cellular signaling. *PLoS Genet* **9**, e1003675 (2013).
39. Nedialkova, D. D. & Leidel, S. A. Optimization of codon translation rates via tRNA modifications maintains proteome integrity. *Cell* **161**, 1606–1618 (2015).
40. Singhal, A., Li, B. T. & O'Reilly, E. M. Targeting KRAS in cancer. *Nat. Med* **30**, 969–983 (2024).
41. Li, M. L. et al. Discovery of novel coumarin-quinolinium derivatives as pan-KRAS translation inhibitors by targeting 5'-UTR RNA G-quadruplexes. *J. Med Chem.* **67**, 1961–1981 (2024).
42. Fujimura, K., Wang, H., Watson, F. & Klemke, R. L. KRAS oncoprotein expression is regulated by a self-governing eIF5A-PEAK1 feed-forward regulatory loop. *Cancer Res* **78**, 1444–1456 (2018).
43. Lampson, B. L. et al. Rare codons regulate KRas oncogenesis. *Curr. Biol.* **23**, 70–75 (2013).
44. Zaki, M. H. et al. The NOD-like receptor NLRP12 attenuates colon inflammation and tumorigenesis. *Cancer Cell* **20**, 649–660 (2011).

Acknowledgements

This work was supported by grants from National Natural Science Foundation of China (82372727 and 82073110 to X.G.; 82470913 to S.W.; 32400980 to S.Y.), and Zhejiang Provincial Natural Science Foundation of China (LZ23H160003 to X.G.). We thank Jiajia Wang and Xiaoli Hong from the Core Facilities, Zhejiang University School of Medicine for their technical support.

Author contributions

Y.Q. and C.W. performed the majority of experiments. S.W., S.Y., and L.Y. assisted with the molecular experiments. X.G., J.P., and Y.G. performed the data analysis. Z.C. and J.Z. assisted in the data analysis. J.H. and W.Y. performed the immunohistochemistry experiments. X.G. conceived the project and wrote the manuscript. All authors discussed the results and edited the manuscript.

Competing interests

The authors declare no competing interests.

Additional information

Supplementary information The online version contains supplementary material available at https://doi.org/10.1038/s41467-025-64144-0.

Correspondence and requests for materials should be addressed to Zhanghui Chen, Jun Zhang or Xiangwei Gao.

Peer review information *Nature Communications* thanks Alain Chariot, Pierre Close and the other anonymous, reviewer(s) for their contribution to the peer review of this work. A peer review file is available.